Applications of the Abbe Sine Condition in Multi-Channel Imaging Systems

Barbara Kruse, University of Arizona, College of Optical Sciences

May 6, 2016

Abstract

In multi-channel imaging systems, having an array of sub-apertures, the particular orientation and alignment between channels must be correct to achieve coherent imaging. The Sine Condition Test (SCTest), developed to identify linear field dependent aberrations (LFDA) to determine the state of alignment of an optical system[1], can be used to align multi-channel systems, and can identify particular LFDA resulting from a relative misalignment between channels, which degrades coherent imaging quality.

Seidel coefficients and Zernike polynomials, which model aberrations in axisymmetric systems across a circular aperture, are not defined across an array of multiple apertures[2]. To design a SCTest for a multi-channel system, pupil mapping error (PME), measured directly from ray trace data, may be used to calculate LFDA. This report derives the mathematical relationship between PME and LFDA, discusses LFDA of special concern in multi-channel imaging systems, and demonstrates the computational toolkit developed to predict LFDA on a dual channel system.

Background

Multi-channel imaging systems combine multiple identical channels coherently to achieve resolutions equal to much larger single channel systems. This coherent combined imaging is highly sensitive to the relative alignment between channels. The SCTest, developed by Burge et al.[3] applies the principles of the Abbe Sine Condition to determine the state of alignment of a given system. A practical advantage of the Sine Condition Test is that it can be performed with respect to the system-defined zero axis, so that test equipment needn't be moved into various field positions for additional measurements.

A system that satisfies the Abbe Sine Condition will by definition be free of linear field dependent aberrations (LDFA). However, many systems fall short of the ideal, if only by a small amount. Pupil mapping error (PME) is one measure of how much the Abbe Sine Condition is violated, one that can be directly mapped to the resulting LFDA.

The design of a Sine Condition Test requires an accurate method to predict the LFDA of the system in various states of misalignment. Separating LFDA from other aberrations can be challenging if not using Seidel Coefficients, as the Seidel Coefficients define the aberrations in terms of field dependence and radial and angular pupil position. Zernike Coefficients do not provide information about field dependence. A general polynomial fit could be made if coefficients are determined at a sufficient number of field points, but this may not be practical.

As most optical design tools rely on Zernike or Seidel analyses to determine the aberrations of a design, a more general tool was needed. The computational toolkit presented here uses ray trace data to calculate the LFDA from the PME without the need for symmetry in the system.

Definition of Pupil Mapping Error

The traditional expression of the Abbe Sine Condition for finite conjugates,

$$\frac{sin\theta_{object}}{sin\theta_{image}} = magnification, \qquad [1]$$

defines a constant ratio of the angles for any given ray travelling from the on-axis object point, O, to its conjugate image point I, also on the reference axis.

It should be noted that the evaluation of the Abbe Sine Condition (SC) does not require that the reference axes be the same in object and image space. The observation points O and I must lie on the reference axes for finite conjugates and point O must be well imaged to I to fulfill the SC. This may seem trivial for axisymmetric systems, as the reference axis for both object and image space is typically defined as the axis of symmetry, but for a non-symmetric system, the definition of the reference axes becomes more complicated. This distinction is made to emphasize that the SC can only be met within a specific coordinate system. A system that fulfills the Abbe SC in one set of reference coordinates, almost certainly will not fulfill the SC in a different set. This behavior is used to identify misalignment, as a system that should show no LFDA, will show them if misaligned from the test reference coordinates.

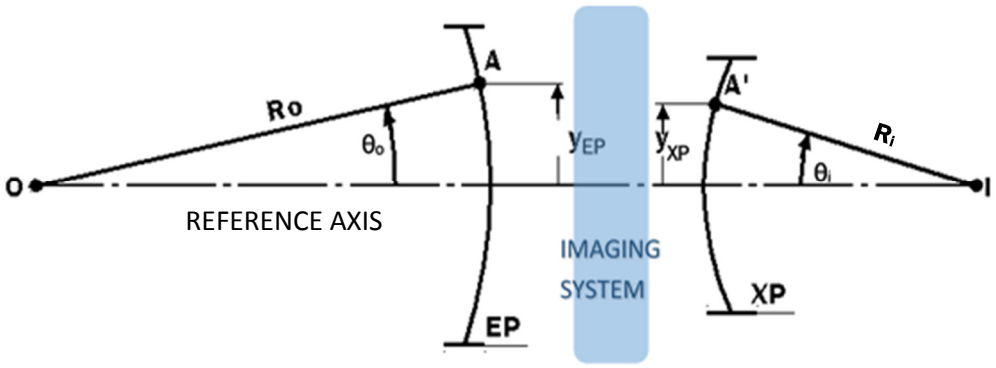

Figure 1 - Object and image space pupil surface definitions for sine condition derivations. For this system,the radius of curvature of the entrance pupil,R_o, is negative.

Although the Abbe Sine Condition can be evaluated at any location, evaluating in the entrance and exit pupils allows the angular relationship to be defined in terms of pupil coordinates. Figure 1 shows the definition of the SC for a finite conjugate pair, defined by points O and I on the axis of symmetry, which is the common reference axis. To maintain the ratio of angles, each exit pupil (XP) coordinate must be a scaled value of its entrance pupil (EP) conjugate. This scale is defined as the pupil magnification, m_P, where:

$$\frac{y_{EP}/_{-R_o}}{y_{XP,ideal}/_{-R_i}} = \frac{y_{EP}/_{-R_o}}{m_P y_{EP}/_{-R_i}} = m \quad so\ that \quad m_P = \frac{R_i}{mR_o} \qquad [2]$$

The pupil magnification, m_P, differs from the paraxial magnification, m. Pupil magnification is the paraxial magnification of the pupil conjugate planes. Note both the entrance pupil and exit pupil

surfaces are not planar, but spherical surfaces with radii of R_o and R_i respectively, as pupils as well as the principal "plane" surfaces all have finite curvature when modelled outside the paraxial regime. For this derivation, the sign of the radii follow standard optics sign conventions. In Figure 1, the radius of the entrance pupil is negative and the radius of the exit pupil, positive.

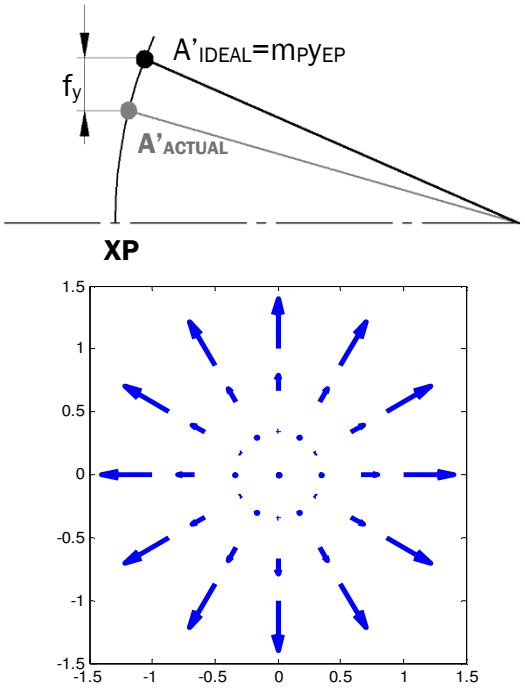

Figure 2- Pupil Mapping Error: Above – graphical representation of pupil mapping error definition. Below -Matlab generated quiver plot of Pupil Mapping Error, f_{PME} for a spherical lens.

When a system satisfies the SC, there will be no LFDA. If it does not satisfy the SC, there will be pupil mapping error. The overall magnification of the pupil, m_P, may be wrong as well as distortion magnification errors which vary with pupil radius. At a given conjugate, some finite distance can be measured between the actual XP coordinate and the ideal. This vector $f_{PME} = (f_x, f_y)$ is continuous across the pupil but can be sampled to create a map of the pupil mapping error (PME) as a function of pupil position, $f_{PME}(\rho_x, \rho_y)$, as seen in Figure 2.

$$f_x = x_{XP,ideal} - x_{XP,actual}$$
$$= m_P x_{EP} - x_{XP,actual}$$

and
$$f_y = y_{XP,ideal} - y_{XP,actual}$$
$$= m_P y_{EP} - y_{XP,actual} \qquad [3]$$

Estimating Linear Field Dependent Aberrations from Pupil Mapping Error – Finite Conjugate[4]

An alternate description of the Abbe Sine Condition is that it guarantees, to the first order, equal optical path lengths through the system. To distinguish the LFDA from other field dependent aberrations, the first derivative relationship, $\partial OPD/\partial h$, between changes in optical path length and field is needed.

As seen in Figure 3, let $\overrightarrow{\varepsilon_o}$, define a very small change in field. The optical path length increases (or decreases) from coordinate point ε_o (at the tip of vector $\overrightarrow{\varepsilon_o}$) to point A, chosen at an arbitrary location on the entrance pupil,

$$OPD_{objectspace} = \overline{\varepsilon_o A} - \overline{OA}$$

$$OPD_{imagespace} = \overline{A'\varepsilon_\iota} - \overline{A'I} \qquad [4]$$

For the slope of $\partial OPD/\partial h$ to be zero, the OPL of the ray travelling from point O to I, through points A and A', must be equal to the same ray travelling from the tip of the field vector, $\overrightarrow{\varepsilon_o}$, through points A and

A', to its conjugate image field, $\overrightarrow{\varepsilon_i}$. For this very small change in field, Fermat's principle guarantees that the path length AA' is stationary and the path length constant, so that

$$W_{LFDA}(h,\rho_x,\rho_y) = h\left(\frac{\partial OPD_{objectspace}}{\partial h}(\rho_x,\rho_y) + \frac{\partial OPD_{imagespace}}{\partial h}(\rho_x,\rho_y)\right) \qquad [5]$$

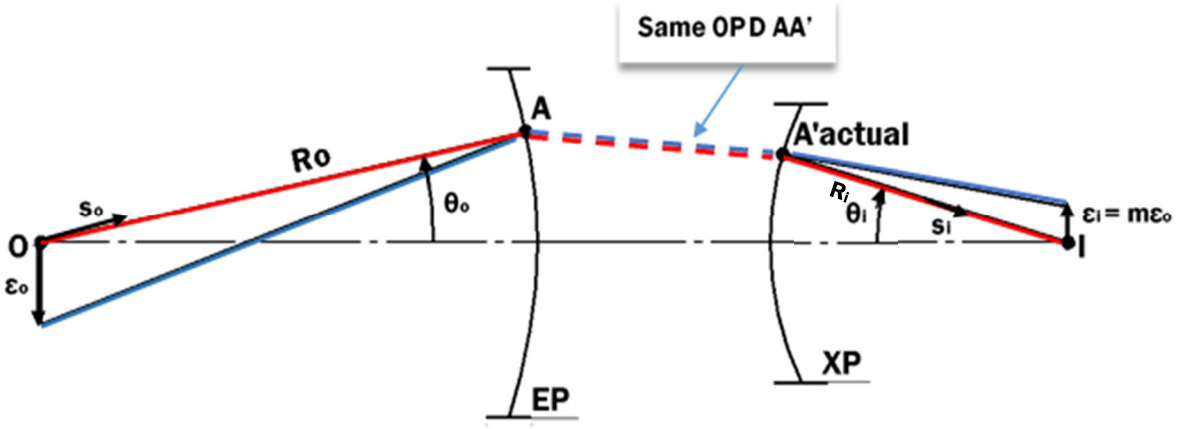

Figure 3- The linear field dependence is determined by finding the change in optical path lengths through common pupil position, point A. For there to be no LFDA at pupil postion A, the total length of the blue lines from object plane to image plane must equal the path length of the red ray, as the magnitude of field vector, $\overrightarrow{\varepsilon_o}$,

For a differential (very small magnitude) field vector, $\overrightarrow{\varepsilon_o}$, any increase in the optical path length from the field in the object plane to the entrance pupil must see an equivalent decrease in optical path length in the path from exit pupil to imaging plane to result in zero LFDA.[*4] Figure 3 graphically represents this relationship, where the total OPL from object to image plane should be equal along both the red and blue paths.

$$\overline{\varepsilon_o A} - \overline{OA} = -(\overline{A'\varepsilon_i} - \overline{A'I}) \qquad (for\ no\ LFDA\ at\ points\ A, A', OPD = 0) \qquad [6]$$

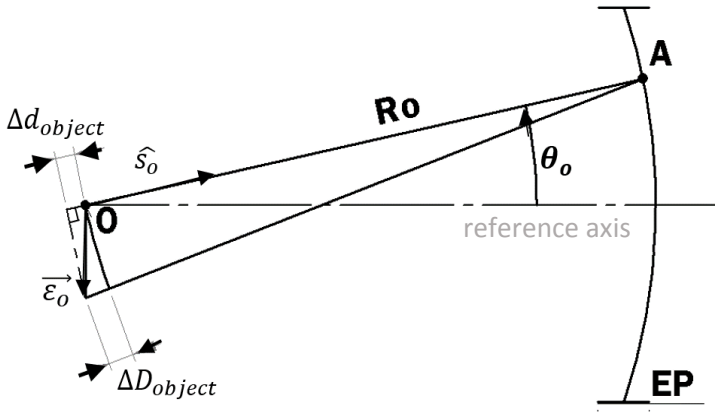

Figure 4- Approximation of the Change in Optical Path Length in Object Space

[*] For this axisymmetric finite conjugate system, the optical path length of the chief ray (passing through the center of each pupil on the axis of symmetry) will increase in both object and image space with increasing field. The magnitude of the OPD increases quadratically with field, therefore the gradient at $\overrightarrow{\varepsilon_o} = 0$ is zero as well as the LFDA.

Figure 4 shows the method for approximating the OPD in object space for small values of $\overrightarrow{\varepsilon_o}$. The change in *OPL,* ΔD, is estimated using a dot product, where $\Delta D \approx \Delta d$:

$$\Delta D_{object\ space} = \overline{\varepsilon_o A} - \overline{OA} \quad \approx \quad \Delta d_{object} = \overrightarrow{\varepsilon_o} \cdot \hat{s_o} = -\varepsilon_{o,x} \sin\theta_{o,x} - \varepsilon_{o,y} \sin\theta_{o,y}$$

$$\Delta D_{image\ space} = \overline{A'\varepsilon_i} - \overline{A'I} \quad \approx \quad \Delta d_{image} = \overrightarrow{\varepsilon_i} \cdot \hat{s_i} = \varepsilon_{i,x} \sin\theta_{i,x} + \varepsilon_{i,y} \sin\theta_{i,y} \qquad [7]$$

where unit vectors $\hat{s_o}$ and $\hat{s_i}$ are defined along the directions of the ray, along $\overline{OA}$ and $\overline{A'I}$, and angles θ_o *and* θ_i are their respective angles with the each reference axis.

Substituting:

$$\overrightarrow{\varepsilon_i} = m\overrightarrow{\varepsilon_o}, \qquad \sin\theta_{o,y} = \frac{y_{EP}}{-R_o} \quad \text{and} \quad \sin\theta_{i,y} = \frac{y_{XP}}{-R_i}$$

$$W_{LFDA,y} = \varepsilon_{o,y}\frac{y_{EP}}{R_o} - m\varepsilon_{o,y}\frac{y_{XP}}{R_i} \qquad [8]$$

If the system does *not* fulfill the Abbe sine condition:

$$y_{XP} \neq m_P y_{EP}\ (ideal\ coordinate) \qquad y_{XP} = m_P y_{EP} - f_y$$

Where f_y is the pupil mapping error, defined in Equation 3.

$$W_{LFDA,y} = \varepsilon_{o,y}\frac{y_{EP}}{R_o} - \left(m\varepsilon_{o,y}\frac{m_P y_{EP}}{R_i} - m\varepsilon_{o,y}\frac{f_y}{R_i}\right)$$

Substituting the derivation for pupil magnification from Equation 2:

$$\boxed{W_{LFDA,y} = \varepsilon_{i,y}\frac{f_y}{R_i}}$$

Combining with the identical derivation for the x-coordinates

$$\boxed{W_{LFDA} = \varepsilon_{i,x}\frac{f_x}{R_i} + \varepsilon_{i,y}\frac{f_y}{R_i}} \qquad [9]$$

Which defines the relationship between pupil mapping error and LFDA.

Verification with Infinite Conjugate

The same principles apply when deriving the solution for the infinite conjugate case, however field is now defined by angle θ_f, and $\mathrm{R_o}$ goes to infinity. Only a reference axis is needed to define rays in object space. The image space reference point, I, and reference axis are defined the same as before.

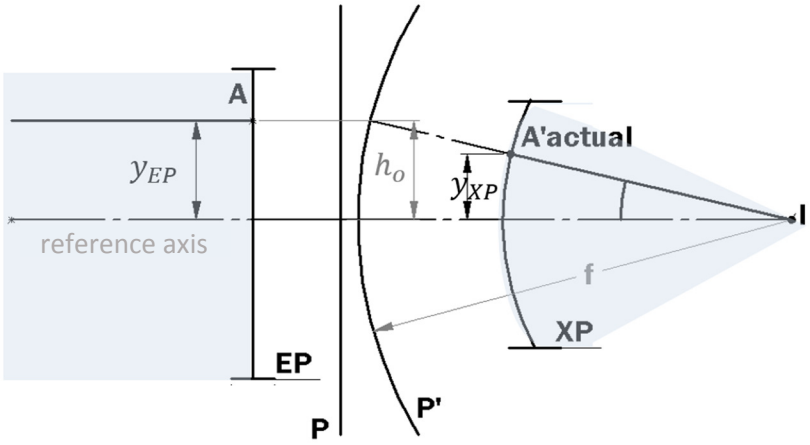

Figure 5 - Infinite conjugate geometry – At a given field angle, all rays enter the entrance pupil are parallel to each other. (θ_f=0 above)

The pupil is now a plane surface ($R_o = \infty$) with a plane wave incident at field angle, θ_f. The change in OPL entering the EP is:

$$\Delta D_{object\ space} = y_{EP} sin\theta_f \qquad [10]$$

which is equivalent to the derivation in the finite conjugate case ($sin\theta_f = {}^{\varepsilon_o}/_{R_o}$, if observed at any

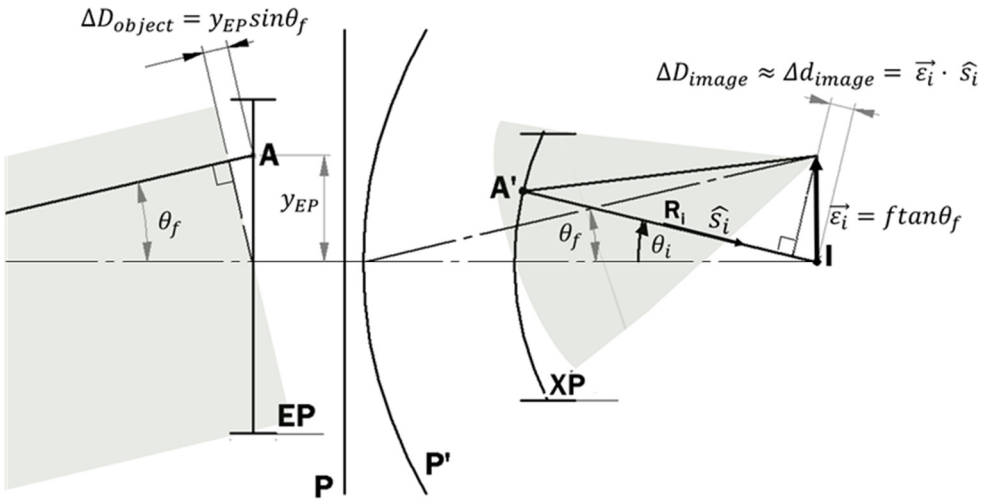

Figure 6 - Definition of Variables for Infinite Conjugate at field angle θ_f

arbitrary plane in object space). For a non-afocal system, there is a converging wavefront, centered at point I, which is also the back focal point of the system.

The same definition for change in optical path length applies as the finite conjugate case.

$$\Delta D_{image\ space} \approx \Delta d_{image\ space} = \varepsilon_{i,x} \sin\theta_{i,x} + \varepsilon_{i,y} \sin\theta_{i,y} \qquad [11]$$

For a field angle defined with no x component:

$$\Delta d_{image\ space} = 0 + \varepsilon_{i,y} \sin\theta_{i,y} = (f tan\theta_{f,y}) \frac{y_{XP}}{R_i}$$

Where f is the focal length of the system and $\vec{\varepsilon_i} = f tan\theta_f$. As can be seen in Figure 5, by the law of similar triangles:

$$\frac{h_{o,y}}{f} = \frac{y_{EP}}{f} = \frac{y_{XP,ideal}}{-R_i} \quad or \quad \frac{h_{o,y}}{sin\theta_{i,y}} = f\,, \qquad [12]$$

Which is the standard form of the infinite conjugate expression of the Abbe sine condition.

$$W_{LFDA} = y_{EP} sin\theta_f + (f tan\theta_f) \frac{(y_{XP,ideal} - f_y)}{-R_i}$$

$$= y_{EP} sin\theta_f - (f tan\theta_f) \left(\frac{y_{EP}}{f} - \frac{f_y}{R_i}\right) \qquad [13]$$

For small field angles (small enough that the $\Delta D \approx \Delta d$ approximation holds true):

$$sin\theta_f = tan\theta_f = \theta_f, \qquad \text{and,}$$

$$W_{LFDA} = (f tan\theta_f)\left(\frac{f_y}{R_i}\right) = \varepsilon_{i,y} \frac{f_y}{R_i} \qquad [14]$$

Which matches Equation 9, the derivation for the finite conjugate case.

To demonstrate this relationship, a cemented doublet lens was analyzed and the results, in Figure 8 and Figure 7, show a graphical representation of the relationship between PME and LFDA.

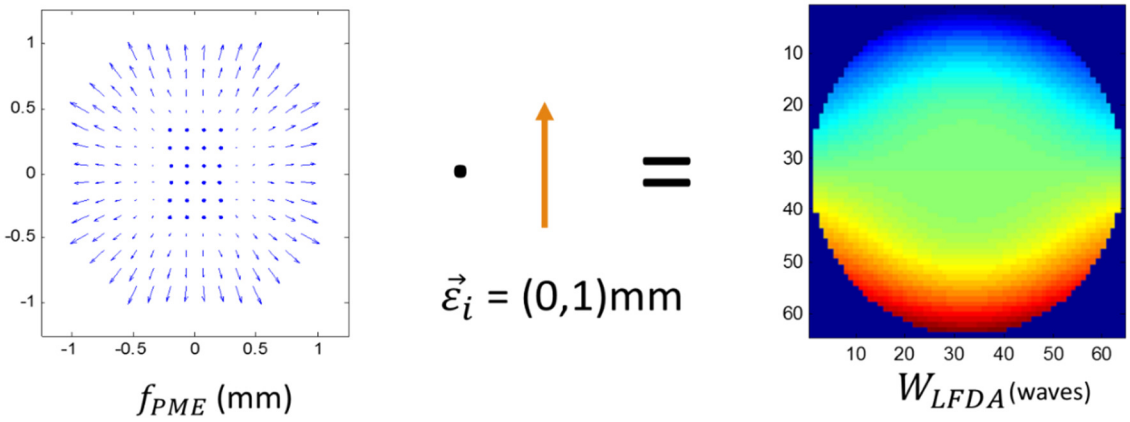

Figure 7 - Matlab generated quiver plot of PME(Left) from an axisymmetric lens doublet. Using the derivation in Equation 9, the dot product of the PME with the field vector in image space (and some scaling) gives the LFDA of the system. This particular lens shows that the dominant LFDA is coma (Right).

The quiver plots on the left show the magnitude and direction of the pupil mapping error at various locations in the pupil. For each pupil coordinate, the dot product was taken with the field vector $\overrightarrow{\varepsilon_i} = (0,1)mm$ and divided by the pupil radius and wavelength to obtain the LFDA. In Figure 8, the same lens was decentered, such that the reference axis was no longer the axis of symmetry. Now, the dominant LFDA is linear field dependent astigmatism.

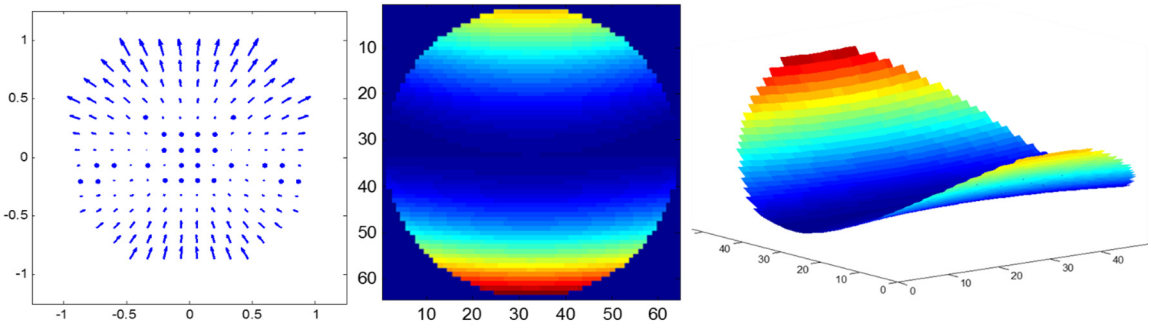

Figure 8 - Quiver plot of PME(Left) and corresponding LFDA (Center and Right) for the same lens in Figure 7, decentered from the optical axis. The presence of linearly (not quadratically) field dependent astigmatism shows that the system is no longer axisymmetric.

Pupil Mapping Error and LFDA of Multi-Channel systems

Multi-channel systems are designed to make use of the increased resolution achieved by the coherent addition of the multiple channels. Figure 9 shows a simplified design for a binocular telescope. Typically, two or more identical channels are aligned in parallel, with fold mirrors for spacing and combination optics to combine the channels together.

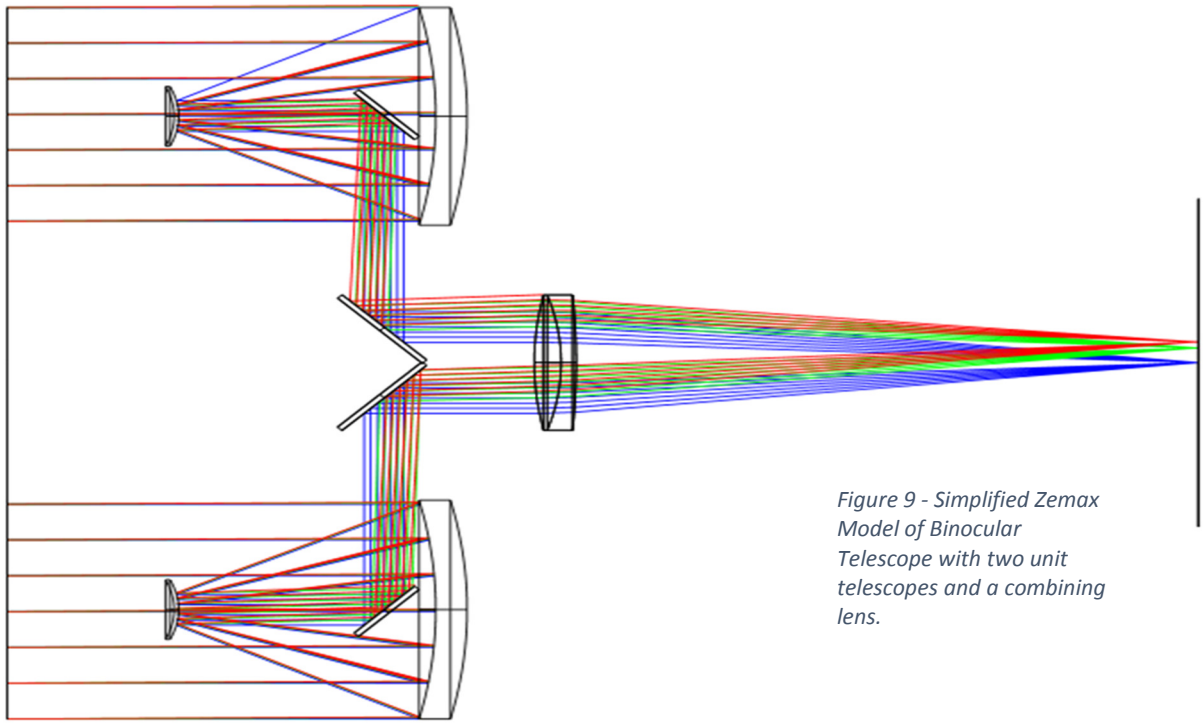

Figure 9 - Simplified Zemax Model of Binocular Telescope with two unit telescopes and a combining lens.

Figure 11 shows the ideal point spread function of a dual channel system, the product of a linear cosine wave defined by the spacing between the channels, and the airy pattern corresponding to the individual sub-apertures. The width of the cosine wave narrows the width of the PSF peak for increased resolution in one direction. Multi-channel systems make use of this same phenomenon with an array of circular apertures, which can improve resolution in more directions. The ability to achieve this improved resolution is greatly determined by the alignment of the channels to one another. To achieve a coherent combination of channels, they must be focused to the same location for all fields and the coherence length of the source must be longer than any optical path length mismatch between

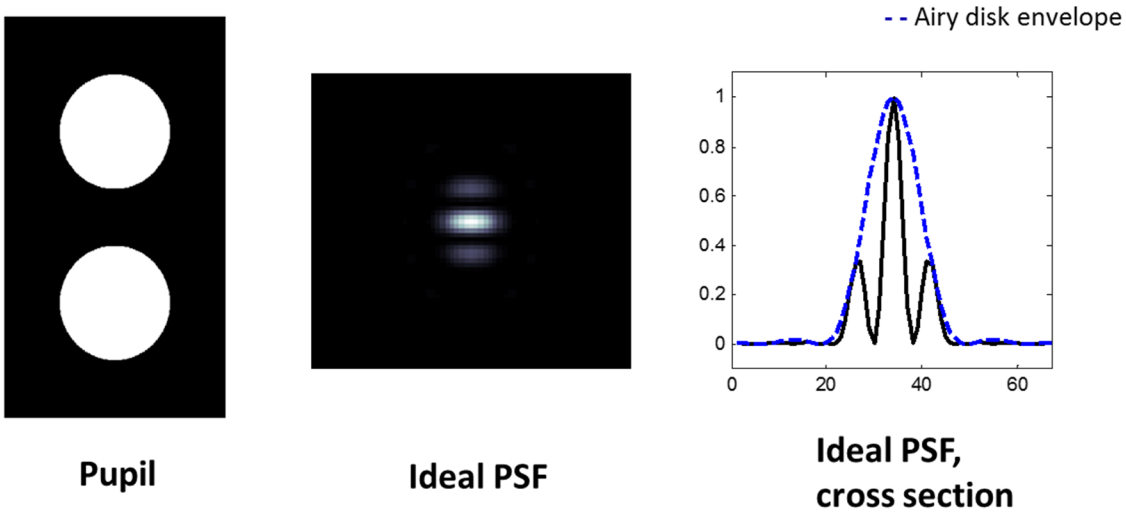

Figure 11 – Pupil of a binocular system (Left) with corresponding ideal PSF (Center) and its cross section (Right). The dotted blue line shows the envelope of the corresponding airy disk pattern of a single centered aperture.

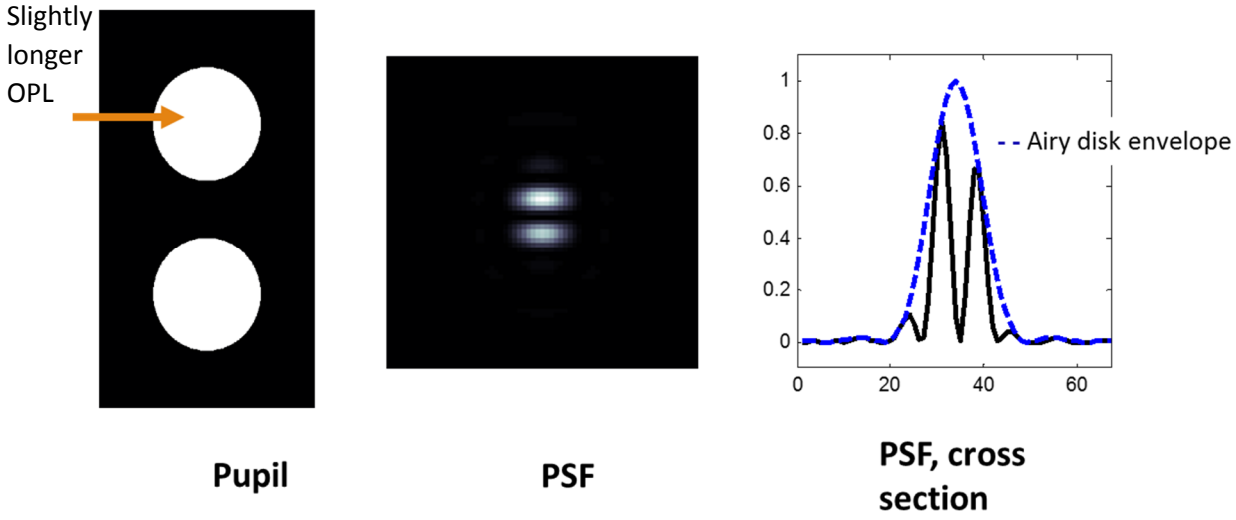

Figure 10 –Identical pupil as Figure 11 with relative piston between pupils (Left) with its corresponding phase shifted PSF(Center), and cross Section(Right). Although the pupil shapes appear identical, the relative piston between the two channels causes the cosine to shift such that it is no longer aligned to the center of the airy peak.

channels. The aberrations of concern in axisymmetric systems still apply to each individual channel, but there are additional aberrations that occur due to relative misalignment of the channels to one another.

Piston, the simplest of the aberrations, is typically ignored in axisymmetric systems- but relative piston between two channels will degrade the coherent imaging as it shifts the phase of the cosine away from the peak of the airy disk. Figure 10 shows the same pupil in Figure 11, with the addition of a piston term in the bottom channel. The cosine term underneath the airy disk envelope, shown with the blue dotted line, is no longer centered on the peak.

This discussion on *constant* relative piston is for explanation only. The Sine Condition Test only identifies *linear* field dependent aberrations, and therefore will not detect relative piston if it is not linearly field dependent. However, both linear field dependent relative-piston and relative-magnification error can be measured using the SCTest to determine the alignment and performance of a multi-channel system.

Relative Magnification Error- Linear Field Dependent Tilt

First order magnification errors in single channel systems can typically be corrected without much difficulty. Fields are imaged in the wrong location in the image plane, however the error is a consistent scaling error across the image. Relative magnification error between channels causes problems as the two channels no longer image to the same point except for zero field angle. The aberration resembles tilt in one pupil and the magnitude increases with field, causing an increasing separation of the PSF centers.

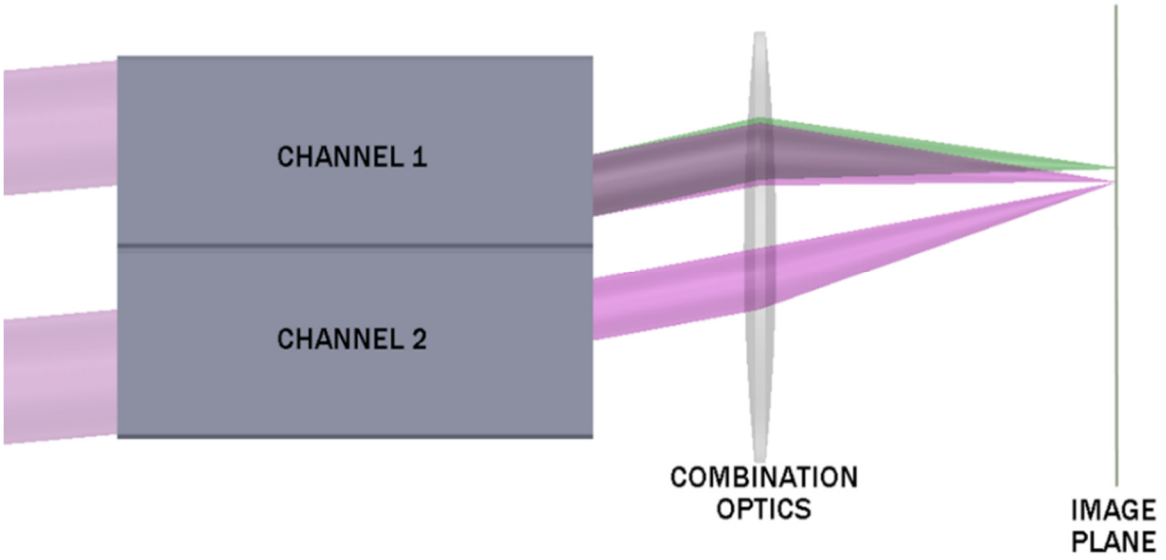

Figure 12- Simplified dual-channel infinite conjugate system showing ideal behavior (purple) and magnification error in Channel 1(green). The ideal channels combine to the same point in the image plane, whereas the green channel focuses to a different point in the image plane.

The PME for a relative magnification error, shows error linearly increasing with radial position in the top pupil, which results in tilt in the corresponding LFDA. Figure 14 outlines the behavior of relative magnification error for three different plane waves of increasing field angle. Though parallel plane waves enter the system, the angle of the corresponding output beams is no longer the same. One beam is tilted with respect to the other. As the tilt increases, the PSF appears to separate into two airy patterns. The bottom PSF depicts the ideal imaging on-axis, with steadily increasing separation with field.

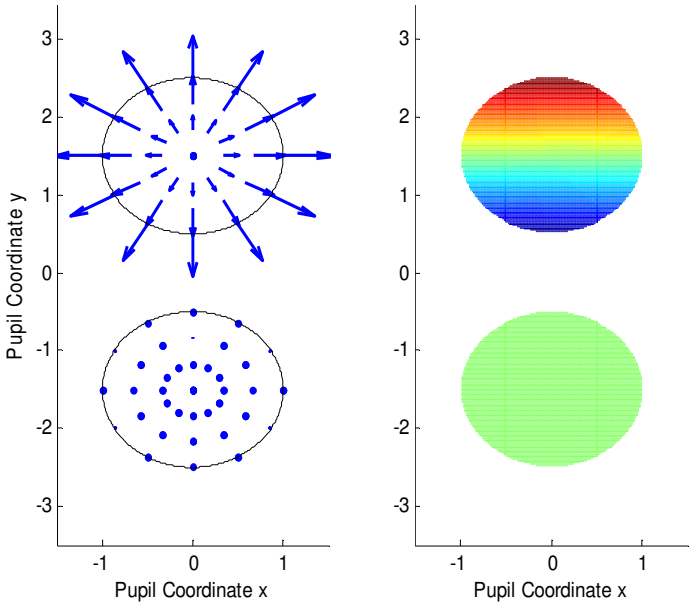

Figure 13 - Pupil Mapping Error (Left) and LFDA(Right) of Dual channel system with magnification error in top channel. LFDA was calculated for a field vector $\vec{\varepsilon_i} = (0,1)mm$

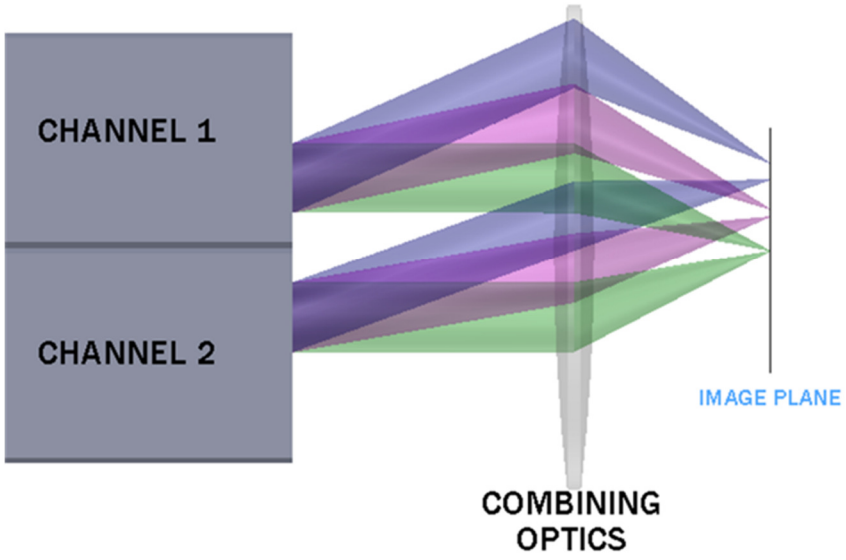

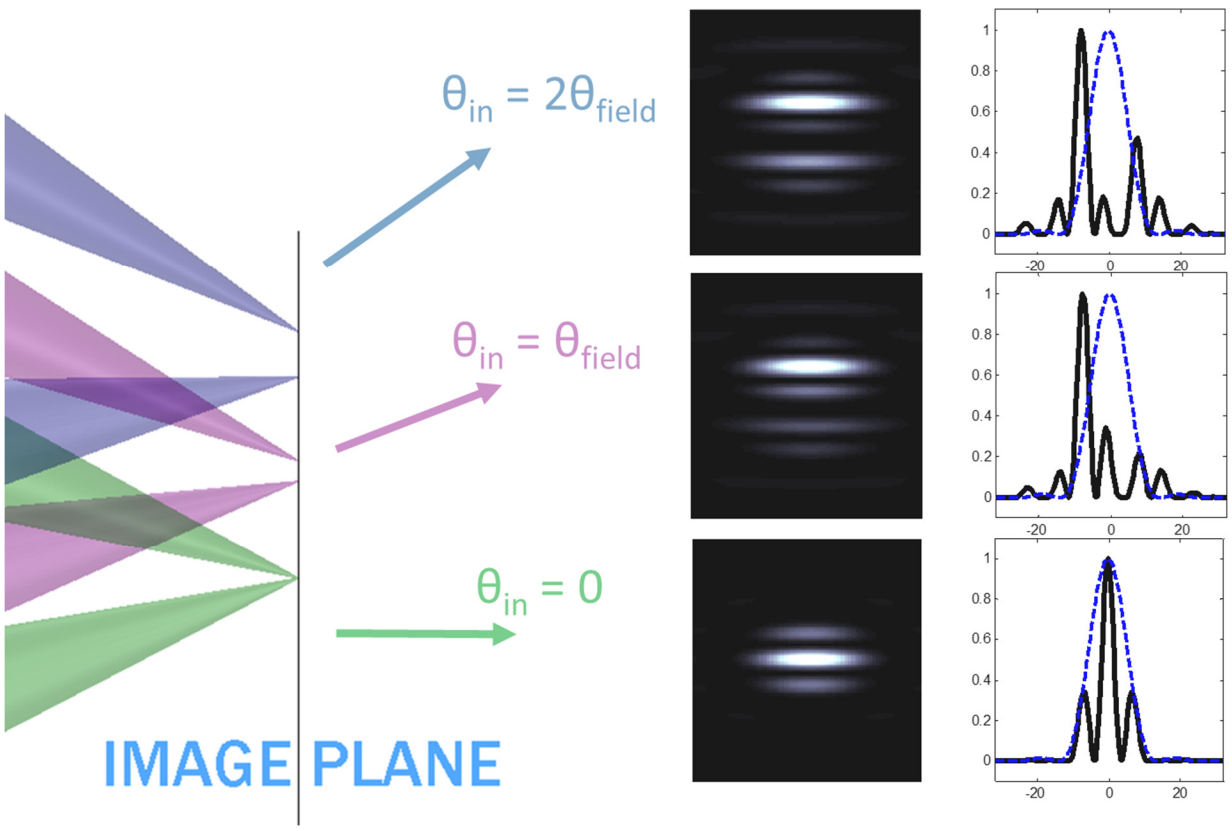

Figure 14- Magnification Error observed at 3 different field angles. The tilt in the top channel causes the focii of the two channels to separate. The blue dotted line in the PSF cross section shows the ideal airy disk envelope. For constant magnification error, but increasing field, the PSF appears to split into two separate airy disks.

Shear – Linear Field Dependent Relative Piston

A multi-channel system could be built of perfectly corrected channels which individually fulfill the SC, yet still violate the sine condition if the relative position of the pupils is not correct. In the SCTest, the entire system pupil is mapped, so the relative position of the channels can be determined. If the distance and orientation between channels is not properly scaled, the pupil mapping error resembles shear, with an error vector of equal magnitude across the entire channel.

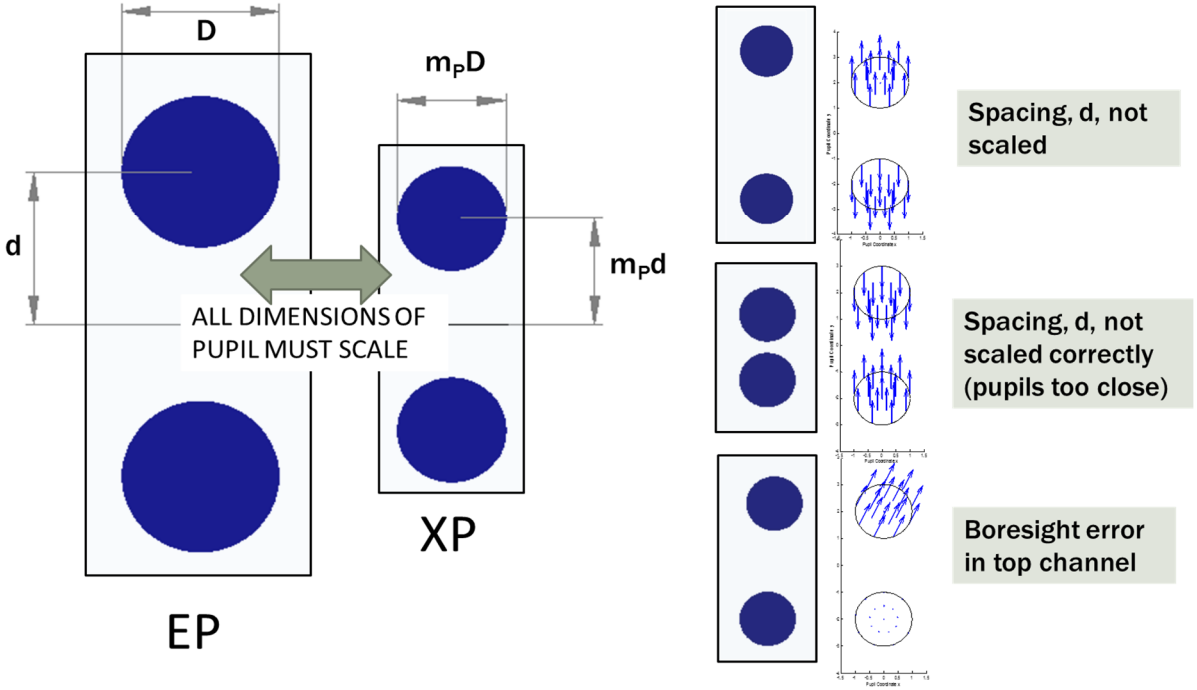

Figure 16 - Examples of scaling and alignment errors between entrance and exit pupils for a two channel system. Pupil alignment errors with their respective quiver plots of pupil mapping error are shown on the right. For all relative positon errors, the PME across the individual channel is constant across the entire sub-aperture.

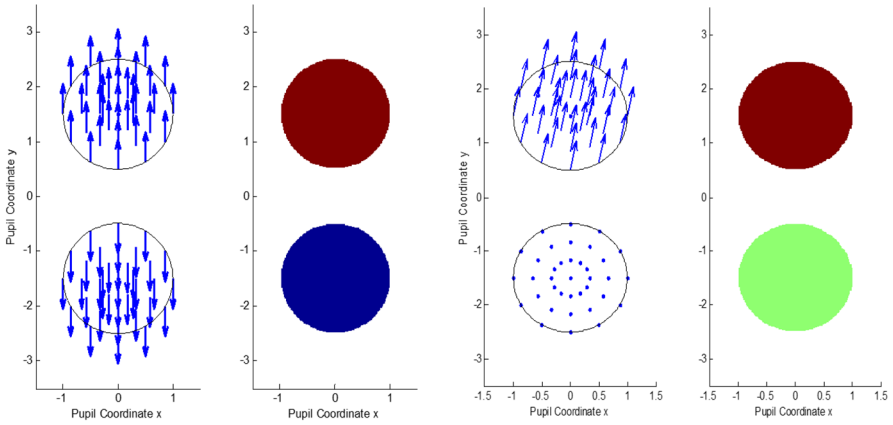

Figure 15 – PME and LFDA for $\varepsilon_i = (0,1)$ for dual channel systems with (Left) incorrect scaling of distance between pupil, (Right) boresight error in top channel. The misaligned pupil positions result in relative piston between the wavefronts, and the magnitude of the piston increases linearly with field.

For a plane wave entering a dual channel afocal system at a given field angle, θ_{in}, the phase difference between rays entering the center of each channel is equal to:

$$\phi_{in,between\ channels} = d_{in} sin\theta_{in} \qquad [15]$$

where d_{in} is the distance between the centers of the two channels. Assuming no aberrations within the channels, a plane wave exits each of the two channels at the correct angular magnification, and the two exiting plane waves are parallel. If the spacing between the exit pupil channels is correct, the phase difference out will exactly equal the phase difference entering the system:

$$\phi_{out,between\ channels} = d_{out} sin\theta_{out} = d_{in} sin\theta_{in} \qquad [16]$$

This holds true only if the Sine Condition is met (no pupil mapping error):

$$\frac{sin\theta_{in}}{sin\theta_{out}} = m = \frac{d_{out}}{d_{in}} \quad or \quad d_{out} = m d_{in}$$

Otherwise, the phase difference between channels is equal to:

$$\phi_{relative-piston} = (d_{out} - m d_{in}) sin\theta_{out} = f_{PME} sin\theta_{field,image\ space} \qquad [17]$$

which is the same form of the equation relating pupil mapping error to LFDA derived previously, if . The resulting PSF from linear field dependent relative piston shows the same shifting cosine wave as discussed for constant relative piston, but that shift is now varying linearly with field.

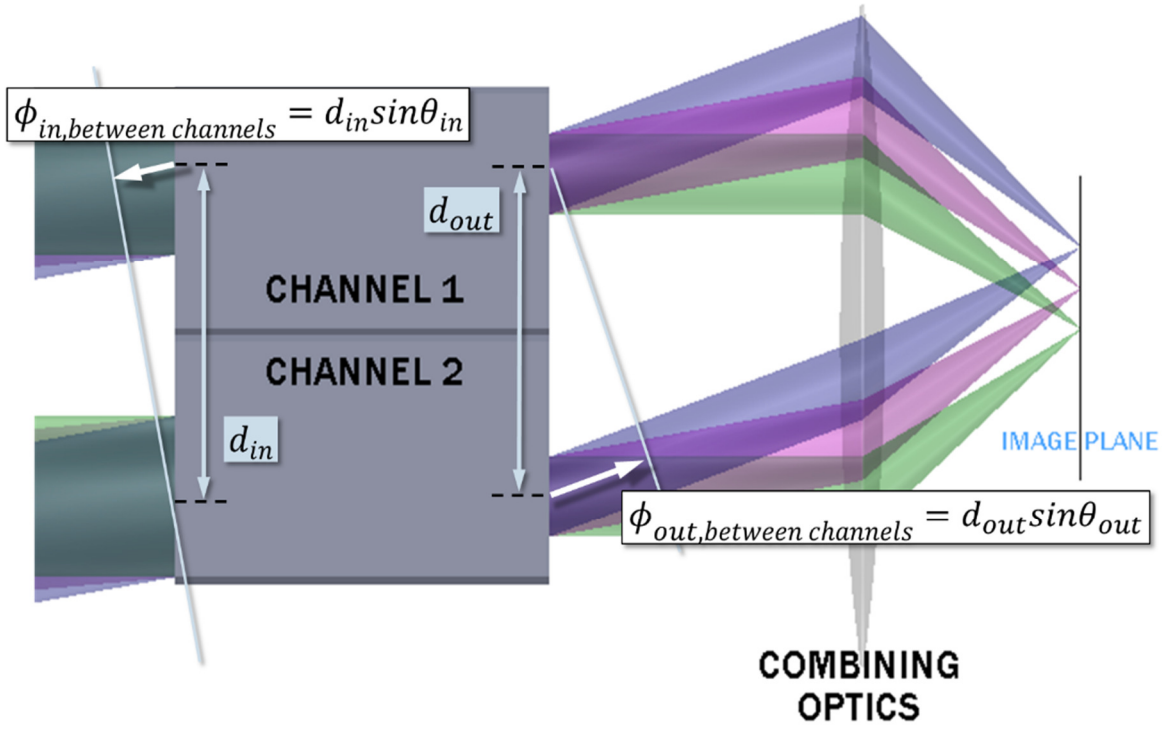

Figure 17- Relative Piston between 2-channels due to incorrect spacing between exit pupils. While the channels combine to same location, there is a piston term between the two channels, which increases with θ_{in}.

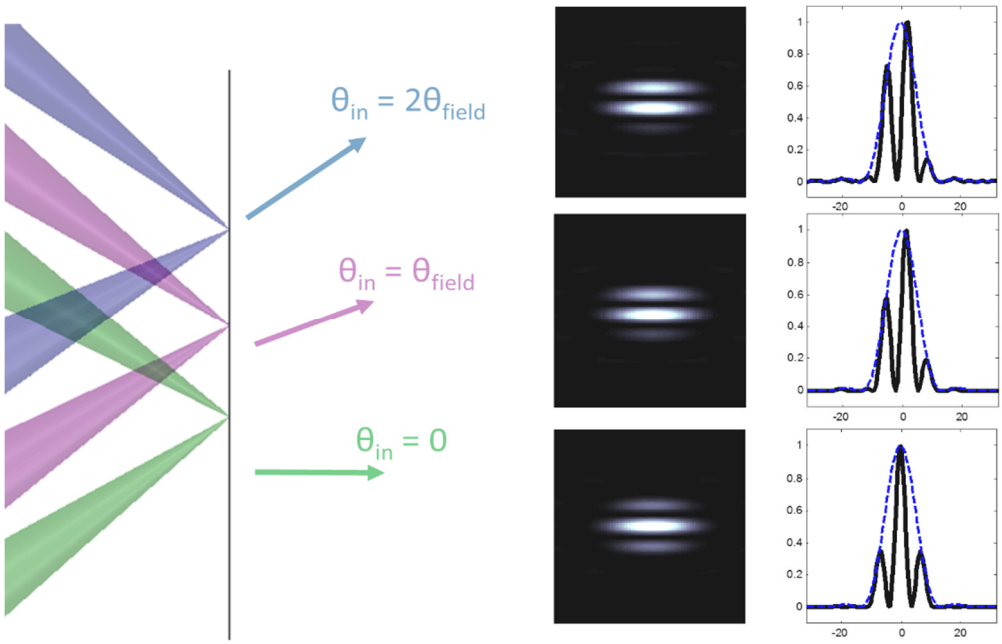

Figure 18- PSFs of a dual channel system with linear field dependent relative piston. The cosine term shifts with field and moves in and out of alignment with the airy disk envelope.

Computational Method for Predicting LFDA from Zemax Models

The purpose of the PME-to-LFDA code is to provide reliable predictions of LFDA for either axisymmetric or non-axisymmetric systems. Pupil mapping error data can be collected using ray trace data from the entrance and exit pupil surfaces. Using the equations derived previously, the data can be used to predict LFDA in designs where Zernike and Seidel Coefficients cannot be reliably calculated.

The matlab script `zPupilMapping.m`[†] makes use of the RAGX and RAGY merit function operands in Zemax to generate a map of the PME as a function of pupil position. The script first queries the entrance pupil coordinates, multiplies by the pupil magnification, m_P, and subtracts this value from the exit pupil coordinates reported from the ray trace. The code allows sampling in either a radial or square sampling grid, and generates a wavefront map of the LFDA, similar to those generated by Zemax.

Verification for Axisymmetric Lenses

For simple axis-symmetric systems, the only predicted LFDA is coma and can be predicted by both Zernike and Seidel Analysis. For Zernike Analysis, linear field dependent coma is calculated as $Z_{LFDCOMA} = 6\sqrt{2}Z_7$, where Z7 is the Zernike Standard Coefficient defined by the equation - 8^(1/2) (3p^3 - 2p) * SIN (A). The second term of the Z7 coefficient is cancelled by the Z3 term if no tilt is present in the system.

[†] All code used in these examples with the supporting Zemax Files are located at https://github.com/kruse/PMEtoLFDA_toolkit.git

The first verification was done on the singlet plano-convex lens from Thorlabs, LA1256, with a nominal focal length of 500mm. Verification was done on 3 finite conjugates and 1 infinite conjugate by varying the location of the conjugates. Table 1 and Figure 19 show the results of the analysis. The variation between LFDA predictions was hundredths of a wavelength for all 4 conjugates.

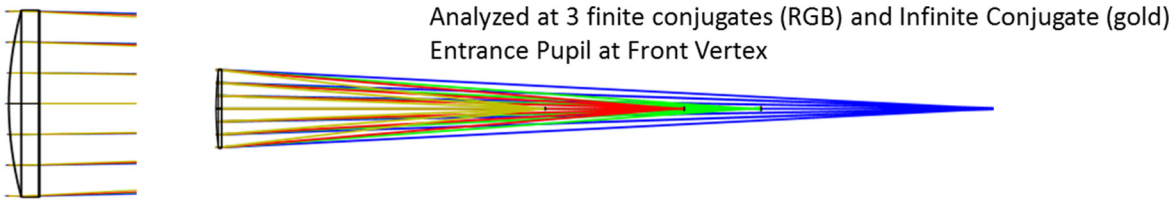

Table 1 – Comparison of LFDA for Single Plano Convex Lens (shown above) at 4 different conjugates

	LENS	Thorlabs LA1256		lambda (nm)	550
			LFDA Predictions		
	object distance,z	field vector, $\boldsymbol{\varepsilon}_i$	PME predicted	Zernike COMA Prediction	Seidel COMA Coeffient W_{131}
units	mm	mm	waves		
Config 1	500	[0,1]	0.41	0.42	0.40
Config 2	750	[0,1]	0.44	0.45	0.43
Config 3	1000	[0,1]	0.41	0.42	0.40
Config 4	Inf	[0,1]**	0.15	0.16	0.15

** $\vec{\varepsilon_i} = f tan\theta_{field}$, for infinite conjugates

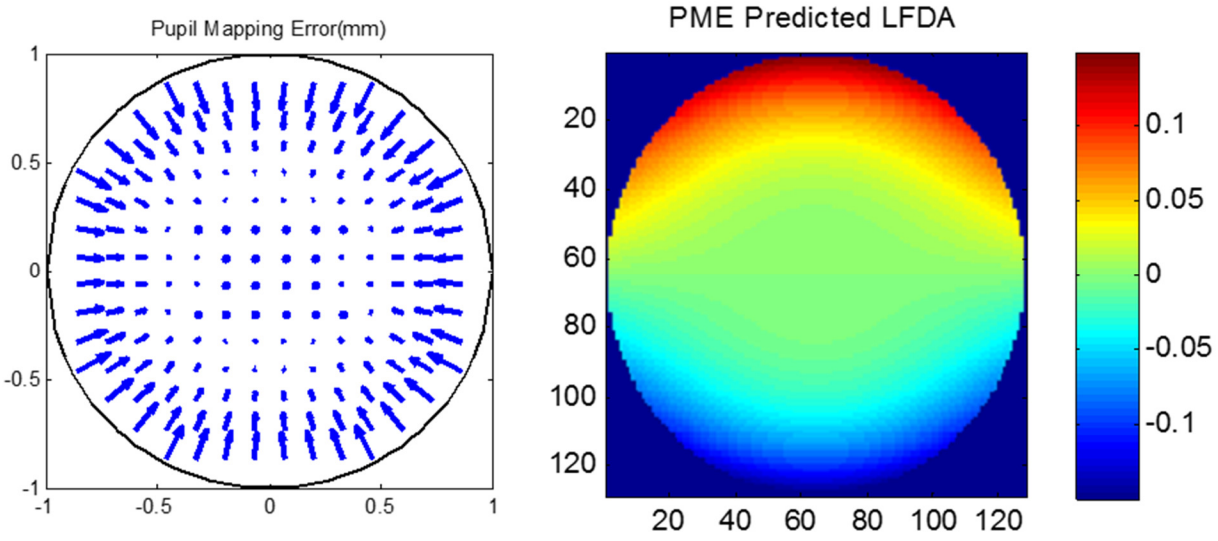

Figure 19- PME quiver plot (Left) and LFDA wavefront (Right) for infinite conjugate of Plano-Convex Lens LA1256

The second axisymmetric verification was done with a cemented doublet, Melles-Griot LAO-300.0-82.0. The analysis methods were identical as the singlet lens, with similar results, as can be seen in Table 2 and Figure 20.

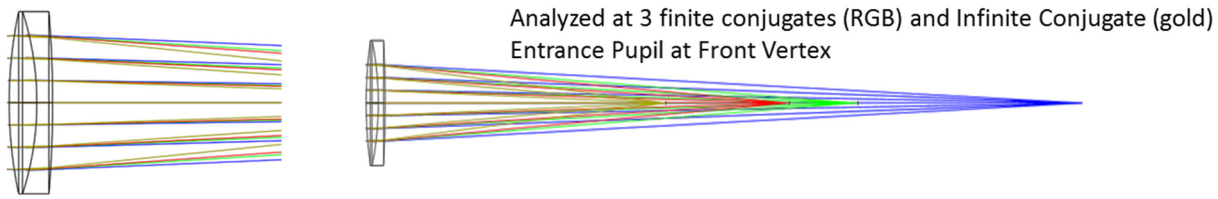

Table 2- Comparison of LFDA Magnitudes for Cemented Doublet Lens (shown above)

	LENS	LAO-300.0-82.0		lambda (nm)	550
			LFDA Predictions		
	object distance,z	field vector, $\boldsymbol{\varepsilon}_i$	PME predicted	Zernike COMA Prediction	Seidel COMA Coeffient W_{131}
units	mm	mm	waves		
Config 1	500	[0,1]	0.16	0.16	0.16
Config 2	750	[0,1]	0.15	0.15	0.15
Config 3	1000	[0,1]	0.13	0.13	0.12
Config 4	Inf	[0,1]**	-0.03	-0.03	-0.03

** $\vec{\varepsilon_i} = ftan\theta_{field}$, for infinite conjugates

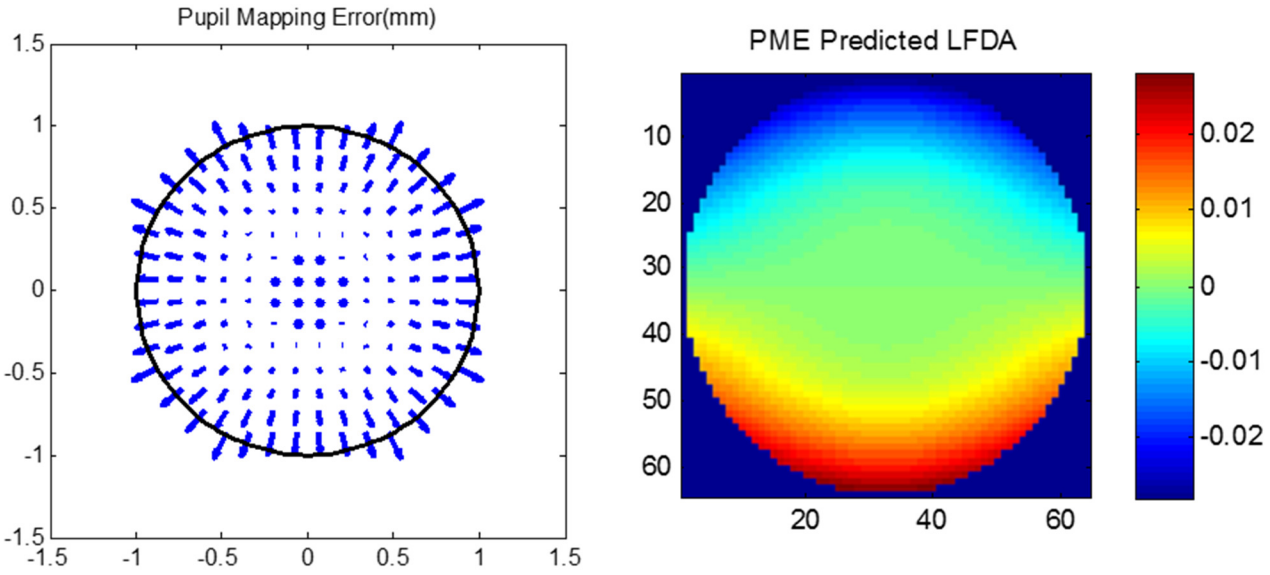

Figure 20 - PME quiver plot (Left) and LFDA wavefront (Right) for infinite conjugate of Melles-Griot Cemented Doublet LAO-300.0-82.0

Analysis of Dual Channel System

Several steps were taken to analyze the dual channel system, pictured in Figure 9, and verify the results were correct with the various changes to the coordinate systems. Starting with a single channel and no fold mirrors, the system was analyzed using the same methods presented in the previous section. The analysis determined virtually no PME was present. The fold mirrors were next included and verified to match the performance by showing no PME.

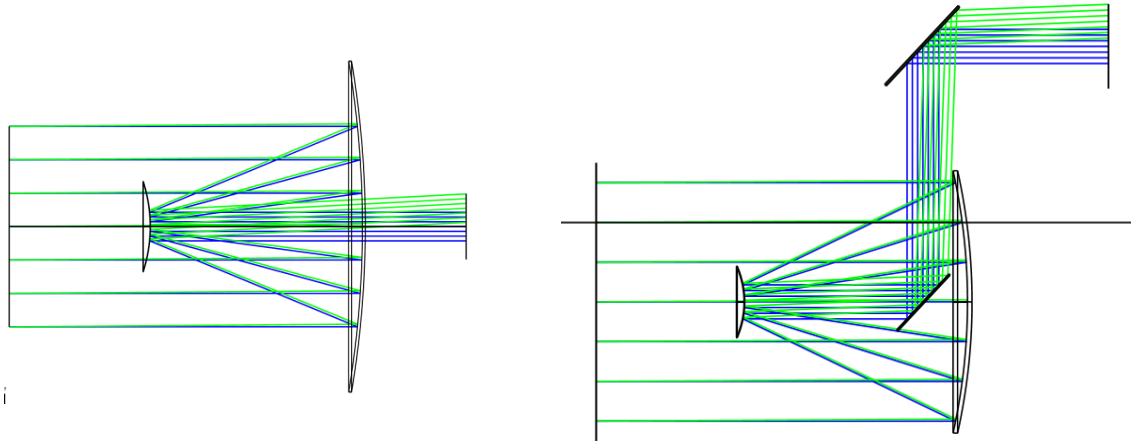

Figure 21- Zemax Models of the Single Channel analyzed by itself. Both systems were found to have zero PME and therefore no LFDA

The combination lens was verified by itself with the aperture stop located identically to the entrance pupil position in the combined system. **Error! Reference source not found.** shows the analysis of the combination lens with 2 circles overlaid to show the sub-apertures of the dual channels.

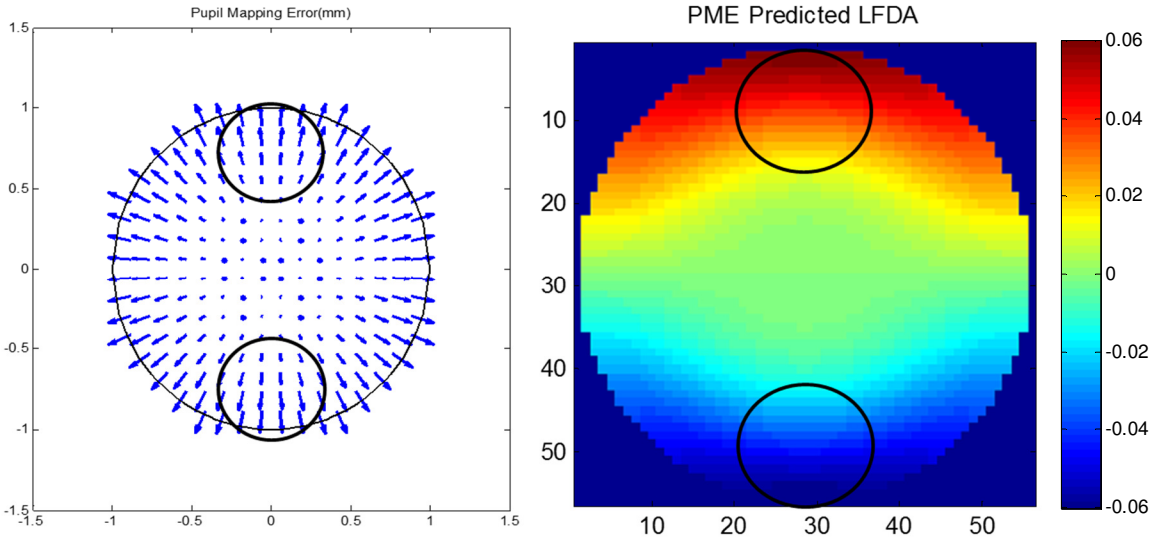

Figure 22 - Analysis of Combination Lens at a field angle of 1mrad. Black circles indicating the location of the 2 sub-apertures of the full systems. By itself, the combination lens shows a small amount of coma

While the shape of the full aperture aberration is dominated by coma, the sampling in the smaller sub-apertures shows relative piston between the two. The final analysis of the full system shows this same behavior, pictured in Figure 23.

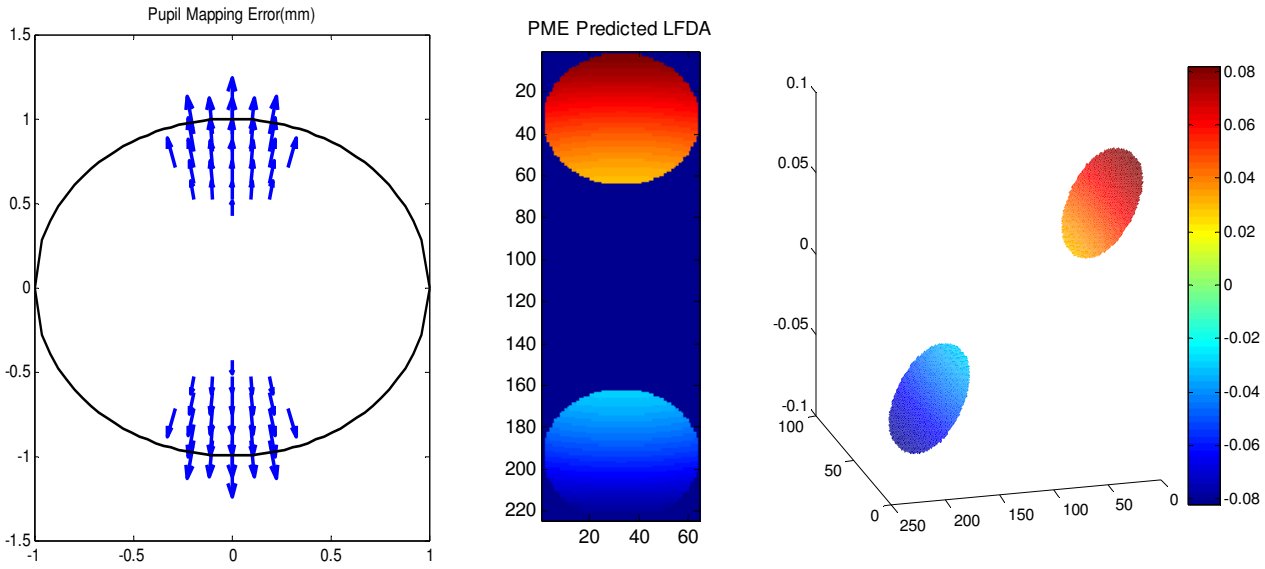

Figure 23 – PME(Left) and LFDA(Center and Right) results for full combined dual channel system observed at a field angle of 1mrad. The two sub-apertures show relative piston between the two as a result of the coma induced by the combination lens

REFERENCES

[1] Dubin, M., Lampen, S., Burge, J. H., "Characterization of alignment using measurements of the sine condition," Proc. SPIE 8131, (2011).

[2] M. Born and E. Wolf, *Principles of Optics* (Pergamon, Oxford, 1975), pp. 464–473.

[3] Burge, J. H., Zhao, C., Dubin, M., Lampen, S., "Determination of off-axis aberrations of imaging systems using on-axis measurements," Proc. SPIE 8129, (2011).

[4] Sara Lampen, Matthew Dubin, and James H. Burge, "Implementation of sine condition test to measure optical system misalignments," Appl. Opt. 50, 6391-6398 (2011)